Applied Catalysis B: Environmental 324 (2023) 122261

Contents lists available at ScienceDirect

Applied Catalysis B: Environmental

journal homepage: www.elsevier.com/locate/apcatb

"On-off" control for on-demand H_2 evolution upon Si-H bond hydrolysis: A combined experimental and theoretical study

Xiang Liu [a,*], Xiaotao Jin [a], Jiaying Yan [a,*], Shuaiwei Fan [a,d,**], Yanlan Wang [b], Didier Astruc [c,*]

[a] College of Materials and Chemical Engineering, China Three Gorges University, Yichang, Hubei 443002, China
[b] Department of chemistry and chemical engineering, Liaocheng University, 252059 Liaocheng, China
[c] ISM, UMR CNRS N° 5255, Université de Bordeaux, 351 Cours de la Libération, 33405 Talence Cedex, France
[d] Department of Physics, Hubei Engineering Research Center of Weak Magnetic-field Detection, China Three Gorges University, Yichang 443002, China

ARTICLE INFO

Keywords:
H_2 evolution
Si-H bond hydrolysis
"on-off"switch
Mechanistic insight
Carbon nanotube-stabilized nanocatalyst

ABSTRACT

Although significant advances are achieved in the exploration of new and high-efficiency catalysts for H_2 production from the hydrolysis of B-H bonds, such as NH_3BH_3 and $NaBH_4$, it is still a severe challenge to explore controllable H_2 evolution upon Si-H bond hydrolysis. Herein, we report unprecedented "on-off"switch of the controlled nanocatalyzed H_2 evolution upon hydrolysis of Si-H bond in tetramethyldisiloxane (TMDS) including mechanistic and DFT studies of this reaction. A series of carbon nanotube-stabilized Pd, Au, Rh, Pt and Ru nanohybrid are utilized as highly efficient nanocatalysts for the controlled H_2 evolution upon Si-H bond hydrolysis. Among them, the optimal Pd/carbon nanotube (CNT) nanohybrid exhibits the highest catalytic performance, with a TOF of 4164 h^{-1}, in H_2 evolution upon TMDS hydrolysis at 30 °C. Kinetic studies including Kinetic Isotope Effect with D_2O and DFT calculations are in favor of concerted Si-H and O-H cleavages in the rate-determining step involving SiO–H–OH hydrogen bonding that facilitates water activation. A new and highly selective "on-off" switch is achieved via a Zn^{2+}/EDTA-2Na system for on-demand H_2 evolution upon Si-H bond hydrolysis; this system proceeds by inhibition and activation regulation of surface-active sites on the catalyst. The detailed physical characterizations (particularly XRD and XPS) and DFT calculations have confirmed that Zn^{2+} ions are bound to the PdNP surface, inhibiting surface-active sites by stereo-electronic interaction, which results in H_2 evolution switch off. H_2 evolution is then switched back on by using EDTA-2Na due to its excellent coordination to Zn^{2+} ions, reactivating these surface-active sites.

1. Introduction

Hydrogen (H_2) has been regarded as one of the most promising and suitable alternatives for fossil fuels due to its superior calorific value, abundant resources, easy accessibility and zero carbon emissions.[1–6] However, it is a matter of extreme urgency to effectively and safely generate, transport and store H_2 gas,[7–12] because of its ultrahigh explosiveness, ultra-low density and dilemma of liquefaction, hindering the industrial and large-scale application.[13–16] To overcome the above issue, significant advances have been achieved in the exploration of new and high-efficiency catalysts for H_2 production from the hydrolysis of B-H bonds, such as $NaBH_4$ and NH_3BH_3.[17–23] There are few available reports on H_2 evolution upon the hydrolysis of Si-H bonds, however.[24–28] For example, in 2016, Kaneda's group first reported Au/HAP catalyzed on-demand H_2 production upon organosilanes hydrolysis. Among them, the "on-off" switch for on-demand H_2 production was realized by the addition and removal of the heterogeneous Au/HAP catalyst.[29] Organosilanes, with Si-H bonds, have recently aroused widespread concern in the safe and effective generation, transportation and storage of dihydrogen gas due to the following advantages: (i) most organosilanes, e.g. TMDS, are common and low-cost byproducts of the silicon industry;[30–32] (ii) the only by-products of H_2 evolution upon hydrolysis of Si-H bond (Eq. 1) are organosilanols that are extensively applied in silicone polymer materials and C-C cross-coupling reactions;[33–35] (iii) most organosilanes are liquid at room temperature and are easily recharged and transported by existing chemical tank trucks.[36–40].

* Corresponding authors.
** Corresponding author at: College of Materials and Chemical Engineering, China Three Gorges University, Yichang, Hubei 443002, China.
E-mail addresses: xiang.liu@ctgu.edu.cn (X. Liu), yanjiaying327@126.com (J. Yan), phyfsw@ctgu.edu.cn (S. Fan), didier.astruc@u-bordeaux.fr (D. Astruc).

https://doi.org/10.1016/j.apcatb.2022.122261
Received 5 October 2022; Received in revised form 28 November 2022; Accepted 3 December 2022
Available online 9 December 2022

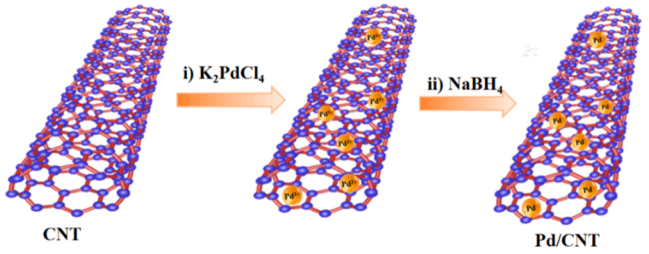

Scheme 1. The synthesis of Pd/CNT.

$$(Me_2SiH)_2O + 2H_2O \xrightarrow{Pd/CNT} [Me_2Si(OH)]_2O + 2H_2\uparrow \quad \textbf{Eq. 1} \quad (1)$$

Herein, we report carbon nanotube-stabilized Pd, Au, Rh, Pt and Ru nanohybrid as highly efficient nanocatalysts, via immobilization of transition metal nanoparticles (TMNPs) onto carbon nanotube (CNT), [41–43] for controllable H_2 evolution upon hydrolysis of Si-H Bond. Among them, the optimal Pd/CNT nanohybrid exhibited the highest catalytic performance, with a TOF of 4164 h^{-1}, in the H_2 evolution upon TMDS hydrolysis at 30 °C. First, the nanostructure and morphology of Pd/CNT has been characterized by Brunner-Emmet-Teller (BET), X-Ray Powder Diffraction (XRD), Fourier Transform Infrared Spectroscopy (FTIR), Raman spectrum, transmission electron microscope (TEM), high resolution TEM (HRTEM), energy dispersive X-ray spectroscopy (EDX) element mapping and X-ray photoelectron spectroscopy (XPS). Then, we scrutinized the catalytic activity and kinetic study of Pd/CNT nanocatalysts in H_2 evolution upon hydrolysis of TMDS, the mechanistic insights into this Si-H bond hydrolysis using kinetic isotope effects (KIEs), cation effect, and density functional theory (DFT) calculations for controllable H_2 release. In addition, an unprecedented and highly selective "on-off" switch for on-demand H_2 evolution upon hydrolysis of Si-H bond is successfully achieved by inhibition and activation regulation of surface-active sites of the catalyst.

2. Experimental section

2.1. Synthesis of Pd/CNT

Typically, 100 mg of commercial carbon nanotube (CNT) and 1 mL of K_2PdCl_4 aqueous solution (0.025 mmol/mL) were dispersed into 9.0 mL of deionized water, and the mixture was stirred for 1 h. Then, 1.0 mL of $NaBH_4$ aqueous solution (including 0.25 mmol of $NaBH_4$) was added to the above solution, and the mixture stirred for 30 min at room temperature. Finally, the black precipitant of Pd/CNT nanocatalyst was isolated by the sample filtration, and washed with deionized water *resp.* EtOH, and dried at 50 °C for overnight.

2.2. H_2 evolution from the hydrolysis of Si-H bond

Generally, 20 mg of Pd/CNT (0.5 mol% Pd) was added into a 10 mL Schlenk flask (water bath at 30 ℃), then 1, 4-dioxane (1 mL) and water (1 mL) were injected into the flask. The flask had been linked, via a gas outlet, into a water-filled glass column. Once 180 μL of 1,1,3,3-tetramethyldisiloxane was injected in this Schlenk flask, and kept a record of the corresponding time and the H_2 gas's volume, simultaneously. The H_2 gas's volume was recorded periodically by recording the volume of H_2O variation in the glass column.

2.3. The "on-off" switch

The "on-off" switch of H_2 evolution from the hydrolysis of Si-H bond had been achieved by adding an equimolar amount of EDTA-2Na and Zn $(NO_3)_2$ aqueous solution. 20 mg of Pd/CNT (0.5 mol% Pd) was added into a 10 mL Schlenk flask (water bath at 30 ℃), then 1, 4-dioxane (1 mL) and water (1 mL) were injected into the flask. Once 360 μL of 1,1,3,3-tetramethyldisiloxane was injected in this Schlenk flask. After 1 min, 2.5×10^{-3} mmol of $Zn(NO_3)_2$ solution was slowly added into the flask and H_2 generation was stopped. After 2 min, 2.5×10^{-3} mmol of EDTA-2Na solution was added into the flask and the H_2 generation was switched on again.

3. Results and discussion

3.1. Compared the hydrolysis of Si-H bond catalyzed by these TMNPs/CNT

As shown in Scheme 1, first, these Pd, Au, Rh, Pt and Ru nanohybrids (Pd/CNT, Au/CNT, Rh/CNT, Pt/CNT and Ru/CNT) were synthesized via a deposition-precipitation method using commercial carbon nanotube (CNT) and K_2PdCl_4, $HAuCl_4$, $RhCl_3$, $PtCl_4$ and $RuCl_3$ dissolved in deionized H_2O, followed by $NaBH_4$ reduction at room temperature, respectively.[44] For the sake of contrast, the catalytic performances of Pd/CNT, Au/CNT, Rh/CNT, Pt/CNT and Ru/CNT in H_2 evolution upon hydrolysis of TMDS were measured (Fig. 1**a**). The results show that Pd/CNT exhibit a higher TOF (4164 h^{-1}) than that of Au/CNT (1128 h^{-1}) in H_2 evolution upon TMDS hydrolysis (Eq. 1), whereas Rh/CNT, Pt/CNT and Ru/CNT are catalytically inactive. Other common supports, including CeO_2, ZrO_2, $CoFe_2O_4$ and ZnO, were then tested for H_2 evolution, Pd/CeO_2, Pd/ZrO_2, Pd/$CoFe_2O_4$ and Pd/ZnO nanohybrids

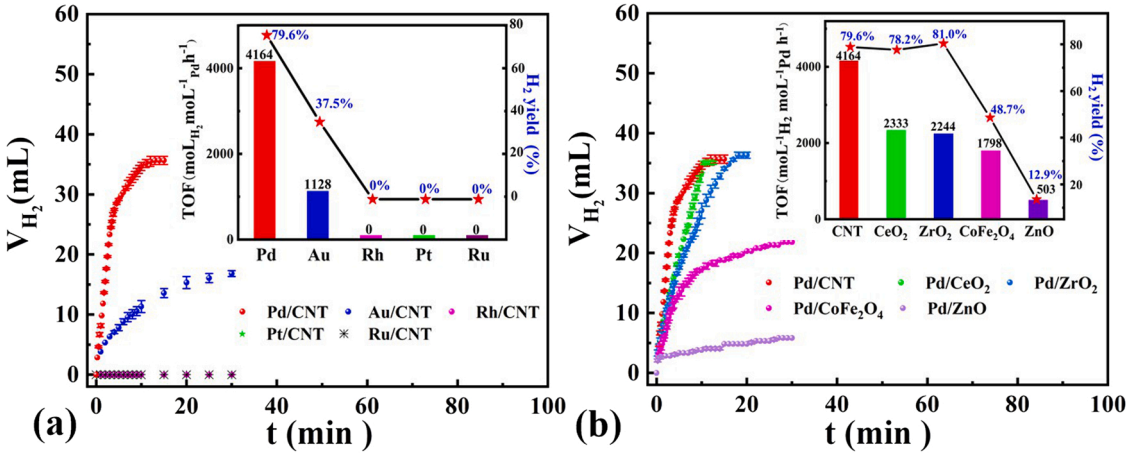

Fig. 1. Comparison of H_2 evolution upon hydrolysis of Si-H bond over 0.5 mol% Pd/CNT, Au/CNT, Rh/CNT, Pt/CNT and Ru/GCN;(b) comparison of H_2 evolution over 0.5 mol% CNT, CeO_2, ZrO_2, $CoFe_2O_4$ and ZnO stabilized PdNPs; Reaction condition:1 mmol of TMDS, 5×10^{-3} mmol of catalyst in the mixture of 1,4-dioxane (1 mL) and water (1 mL) at 30 °C.

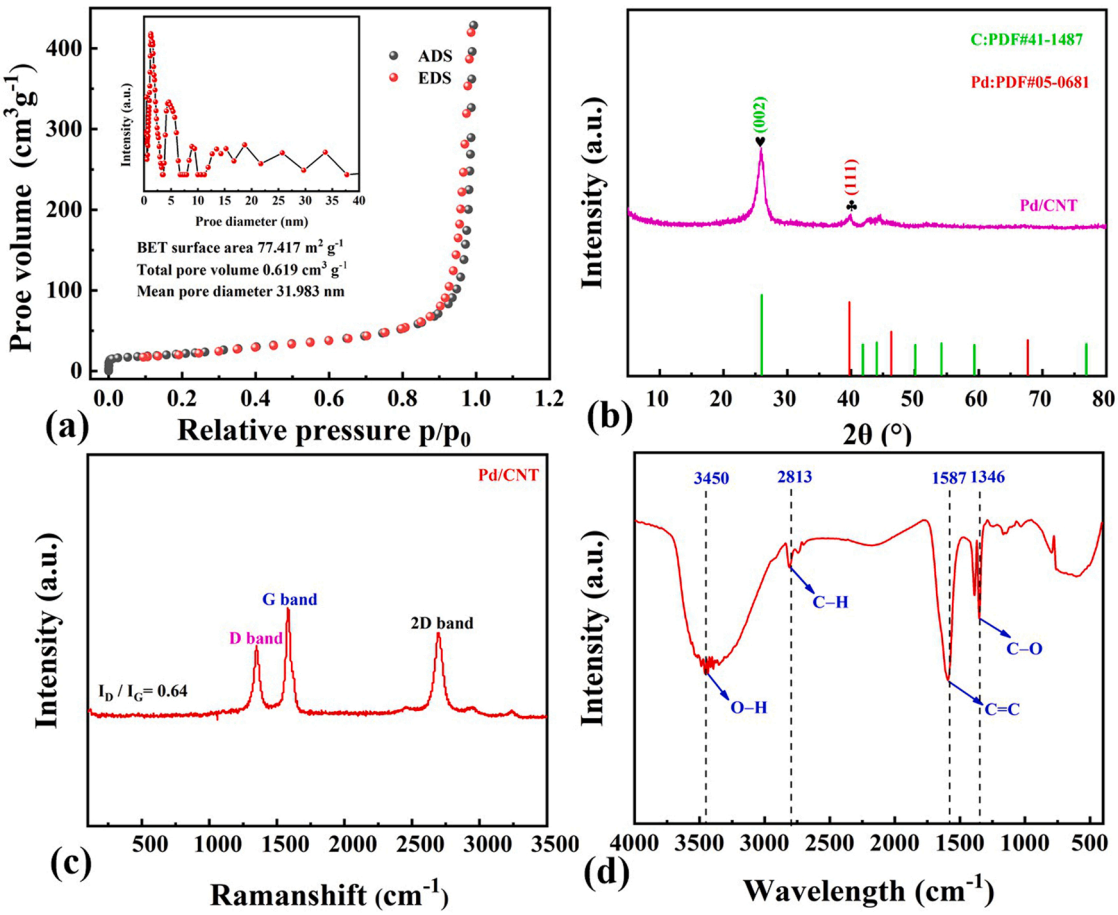

Fig. 2. (a) BET, (b) XRD, (c) Raman spectra and (d) FTIR of Pd/CNT.

were synthesized under standard conditions. In Fig. 1**b**, the order of catalytic activities follows: Pd/CNT (4164 h^{-1}) > Pd/CeO_2 (2333 h^{-1}) > Pd/ZrO_2 (2244 h^{-1}) > $Pd/CoFe_2O_4$ (1798 h^{-1}) > Pd/ZnO (503 h^{-1}). To sum up, Pd/CNT exhibits the highest TOF of 4164 h^{-1} in H_2 evolution, highlighting the vital role of CNT in TMDS hydrolysis.

3.2. *Characterization of Pd/CNT*

In order to explore why Pd/CNT was so efficient in H_2 evolution, the detailed physical characterizations, including BET, XRD, Raman spectra, FTIR, TEM, HRTEM, EDX, ICP and XPS were further measured. As displayed in Fig. 2**a**, the BET result of Pd/CNT nanohybrid exhibited its BET area, average pore volume and average pore diameter of 77.42 m^2/g, 0.62 cm^3/g *resp.* 31.98 nm, suggesting that Pd/CNT present a type II isotherms with H1 hysteresis loops and a standard mesoporous structure.[45] Fig. 2**b** shows a typical sharp peak at 25.8° in the XRD of Pd/CNT, which corresponds to (002) graphene (JCPDS card no. 41–1487).[46] The characteristic peak of Pd (111) at 40° appeared in the XRD (JCPDS card no.05–0681), indicating that PdNPs were immobilized onto carbon nanotubes. In the Raman spectrum of Pd/CNT, the characteristic peaks of the D-band (1351 cm^{-1}), G-band (1585 cm^{-1}) and 2D-band (2703 cm^{-1}) of Pd/CNT were recorded (see Fig. 2**c**). The D-band and G-band are assigned to the disordered carbon and graphite carbon, respectively. The value of I_D/I_G is only 0.64, illustrating that the Pd/CNT only had few defects in the crystal lattices.[47] The FT-IR spectrum was also employed to study the surface functional groups of Pd/CNT, as shown in Fig. 2**d**. The characteristic peaks located at 3450 cm^{-1}, 2813 cm^{-1}, 1587 $cm^{-1}$and 1346 cm^{-1} clearly correspond to the stretching vibration of O-H, C-H, C═O/C═C, and C-O, respectively.[48] These surface functional groups of CNT favor the stabilization of the PdNPs. The surface morphology and structure of the Pd/CNT was further investigated by TEM and HRTEM. As shown in Figs. 3**a and** 3**b**, the Pd nanoparticles, with an average size of 3.57 nm (Fig S1), are uniformly anchored and distributed onto the surface of CNT. Crystal lattice distances of 0.24 nm and 0.37 are clearly observed in the HRTEM of Pd/CNT, corresponding to Pd (111) and C (002), respectively (Figs. 3**c and** 3**d**).[49] These results further confirm that the PdNPs have been successfully stabilized at the surface of the carbon nanotubes. Then EDX elemental mapping of Pd/CNT was further measured in order to investigate the exact position of PdNPs in Pd/CNT (Figs. 3**e**-3**i**). This technique revealed that the total surface of Pd/CNT is composed of C and O, whereas elemental Pd is only distributed in PdNPs, verifying that PdNPs have been successfully stabilized at the surface of the CNT. Fig. 3**f** shows the co-existence of Pd, O and C elements in the EDX sum spectrum, further confirming that a Pd/CNT nanohybrid was successfully synthesized. As shown in Fig. 4**a**, the co-presence of Pd, C and O elements in the Pd/CNT nanohybrid is also verified by the sum XPS spectrum. The high-resolution Pd $3d_{5/2}$ spectra of Pd/CNT is divided into two characteristic peaks at 335.93 eV and 338.12 eV, assigned to Pd^0 (63.35%) and Pd^{II} (36.64%) species, respectively (Fig. 4**b**).[50] This suggests that Pd (0) have been partly oxidized to Pd (II) by air. Fig. 4**c** illustrates that C 1 s spectrum of Pd/CNT is fitted into three typical peaks at 284.84 eV, 286.17 eV and 290. 93 eV, attributed to C═C, C═O *resp.* π-π * . As displayed in Fig. 4**d**, the O 1 s spectrum of Pd/CNT nanohybrid is decomposed into C═O (531.81 eV), C-OH (532.92 eV) *resp.* C-O-C (534.20 eV), further confirming that the CNT's possess abundant reactive surface oxygen species, which is in favor of the stabilization of PdNPs. Furthermore, inductively coupled plasma optical emission spectrometry (ICP-OES) of Pd/CNT indicates that the content of Pd in Pd/CNT is only 2.6 wt%, which is the

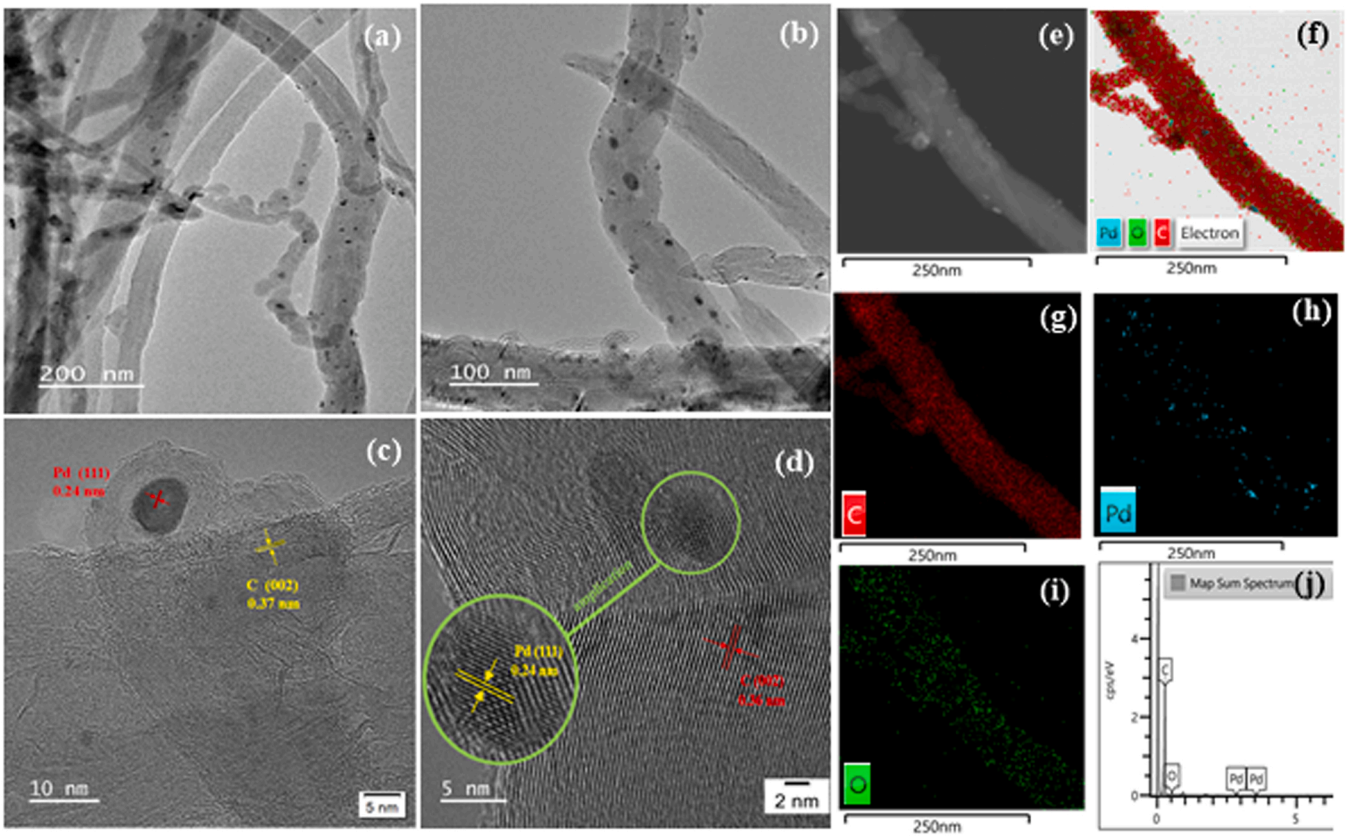

Fig. 3. (a)&(b) TEM, (c)&(d) HRTEM, (e) HADDF-STEM, (f) combined (Pd, O and C), (g) C, (h) Pd, (i) O EDX compositional mapping, and (j) sum spectrum of Pd/CNT.

almost same as the theoretical value. In summary, these results show that the as-synthesized Pd/CNT nanohybrid possesses a nanotube-shaped structure with excellent microporosity, and Pd nanoparticles are successfully immobilized onto CNT.

3.3. Kinetic study on the H_2 evolution upon Si-H bond hydrolysis

Since Pd/CNT nanohybrid exhibits excellent catalytic efficiency in H_2 evolution upon Si-H bond hydrolysis, its further detailed kinetic study was investigated by varying the initial TMDS concentration, the amount of Pd/CNT nanohybrid and reaction temperature upon H_2 evolution. The catalytic activities of H_2 evolution with various initial TMDS concentrations are shown in Fig. 5**a**; the catalytic efficiency increases with the enhancement of concentration of initial TMDS from 0.5 mmol to 2.0 mmol. The initial concentration of TMDS clearly plays a distinct positive role in H_2 evolution. Similarly, an increase in Pd/CNT dosage from 0.1 mol% to 0.7 mol% played a remarkable positive role in H_2 evolution. As displayed in Fig. 5**b**, the slope of catalytic efficiency vs. the amount of Pd/CNT is 2, which indicates that H_2 evolution upon Si-H bond hydrolysis is first order in catalyst concentration. The results of the investigation of the effect of the reaction temperature is shown in Fig. 5**c**. The TOF of H_2 evolution increases from 3092 h^{-1} to 4923 h^{-1} with the increment of reaction temperature (Fig. 5**d**). The activation energy (E_a) of H_2 evolution over Pd/CNT is 21.56 kJ/mol (Arrhenius equation). H_2 evolution upon Si-H bond hydrolysis carried out in D_2O *resp.* H_2O is shown in Fig. 5**e**. A kinetic isotopic effect (KIE) of 1.43 was observed suggesting that the breaking of O-H bond in water is not the major component in the rate-controlling step of the hydrolysis of Si-H bond; on the other hand, it favors a concerted process between Si-H oxidative addition and water O-H bond oxidative addition.[51] As displayed in Fig. 5**f**, the gas chromatograms (GC) also verified that the gas evolution upon the hydrolysis of Si-H bond was only H_2, and the formation of $(Me_2SiOH)_2O$ has also been confirmed by mass spectrum following H_2 evolution (Fig. S2), suggesting that H_2 generation from the hydrolysis of Si-H bond over Pd/CNT is successfully achieved towards fuel cell power systems.

3.4. The mechanism of H_2 generation from Si-H bond hydrolysis

A proposed mechanism of H_2 generation from Si-H bond hydrolysis, based on the above results, is illustrated in Scheme 2. At the beginning, two plausible mechanism pathways (PdSiO–H–OH and.

Pd–H–OH) and the energy change of the cleavage of O-H bond in water are calculated and summarized in Fig. 6. A new PdSiO–H–OH (red route) or Pd–H–OH (blue route) bond could be

formed when H_2O attacked with PdSiO or Pd nanoparticles, the activity energy of red route (24.2 kcal/mol) is much lower than blue route (29.9 kcal/mol), indicating that PdSiO–H–OH bond is more easily formed in the plausible mechanism pathway. Thus, DFT calculation using Gaussian 16 program package [52] has confirmed that the O atom of siloxane forms a hydrogen bond PdSiO–H–OH with water, which weaken the O–H bond of water towards its further oxidative addition on the Pd surface to form Pd-H and Pd-OH species. In the meantime, oxidative addition of the Si-H bonds occurs at the PdNP surface forming Pd-H and Pd-SiO bonds. The KIE of 1.43 with D_2O is much lower than those found upon hydrolysis of $NaBH_4$ and NH_3BH_3 for which water activation is the rate-determining step.[51,53] Thus, it is probable that the low value found here is best taken into account by a concerted process between Si-H oxidative addition and water activation. Indeed, in the cases of $NaBH_4$ and NH_3BH_3 hydrolysis, the preliminary hydride transfer step is fast, because these boron hydrides in which the boron atom bears some negative charges are very hydridic.

Consequently, in these later cases, the hydride transfer step introduces a negative charge onto the Pd surface, much favoring water

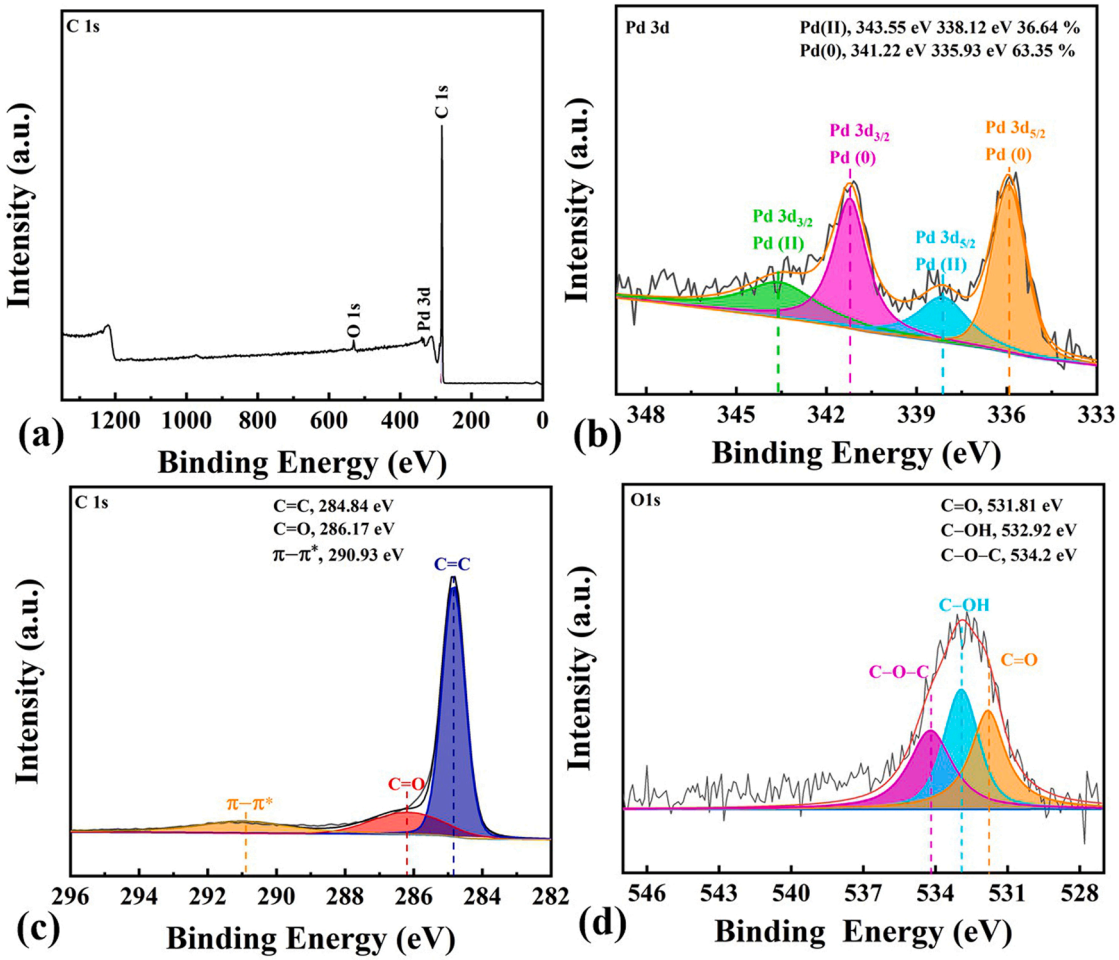

Fig. 4. (a) Sum, (b) Pd 3d, (c) C 1 s and (d) O 1 s XPS patterns of Pd/CNT.

activation. On the other hand, in siloxanes, the Si-O bond is polarized as $Si^{\delta+}$-$O^{\delta-}$, leaving a polarity of the Si-H bond in siloxanes opposite to what it is in boranes. This only leaves the possibility of a simple oxidative addition of the Si-H bond onto Pd without transfer of a negative charge to the Pd surface.

In sum, the only two factors favoring water activation upon siloxane hydrolysis are the water O–H bond weakening by hydrogen bonding indicated above and, synergistically, the attraction of the water molecule nearby the Pd surface upon PdSiO bond formation upon Si-H oxidative addition. Finally, H_2 is released upon reductive elimination of two Pd-H hydrides after "walking" of the two Pd hydride ligands via μ_2-H intermediates near each other at two contiguous Pd atoms.[54] In the meantime, the $[(CH_3)_2SiOH]_2O$ is formed from the reductive elimination of -OH and $[(CH_3)_2Si\text{-}]_2O$ Pd ligands.[28].

3.5. *The "on-off" switch for on-demand H_2 evolution upon Si-H bond hydrolysis*

In order to effectively and safely generate, transport and store H_2 gas, [55–58] the "on-off" switch for on-demand H_2 evolution upon Si-H bond hydrolysis was investigated (Fig. 7). From the above mechanistic studies, the controllable H_2 evolution upon the hydrolysis of Si-H bond should be controllable by the inhibition and activation regulation of the catalytic Pd surface-active sites.[59] First, the"on-off"control condition was optimized using Pd/CNT for H_2 production upon hydrolysis of TMDS as model reaction (Eq. 1). For switching off the H_2 evolution, the corresponding volumes of release H_2 in 2 min from the hydrolysis of Si-H bond over Pd/CNT after the addition of various metal cations (including Pt^{4+}, Ca^{2+}, Au^{3+}, Fe^{3+}, Ag^{+}, Cr^{3+}, K^{+}, Rh^{3+}, Mn^{2+}, Ni^{2+}, Cu^{2+}, Co^{2+}, Ru^{3+} and Zn^{2+}) were recorded (Fig. 7**a**). H_2 evolution was only completely stopped by Zn^{2+} ions, where the released 1 mL of H_2 gas was attributed to the induction time (Zn^{2+} ions moved to the surface of Pd/CNT). To switch back on H_2 evolution, hydrolysis was first completely switched off by Zn^{2+}. Then, the corresponding volume of release H_2 in 2 min was determined from the hydrolysis of Si-H bond over Pd/CNT after the addition of different ligands, including EDTA-2Na, $NaNO_2$, tertiary butanol (BTA), NEt_3, NH_4OH, $NHEt_2$, L-Asp, L-proline, sodium citrate dihydrate (SCTD), urea, and 2-methylimidazole (2-MI) (Fig. 7**b**). These results revealed that H_2 evolution was only completely switched on by EDTA-2Na and that Zn^{2+} selectively and efficiently quenches

H_2 evolution from Si-H bond hydrolysis, while H_2 evolution is reactivated by EDTA-2Na. As shown in Fig. 8, such Zn^{2+}/EDTA-2Na switch was successfully repeated several times without any obvious activity loss in the controllable H_2 evolution upon Si-H bond hydrolysis.

In order to explore the mechanism of Zn^{2+}/EDTA-2Na switch, the XRD of fresh Pd/CNT, Pd/CNT + Zn^{2+} (H_2 evolution was switched off) and Pd/CNT+ Zn^{2+} + EDTA-2Na (H_2 evolution was switched on) were measured (Fig. 9**a**), the typical peak of (002) graphene, located at 25.8° in the XRD of Pd/CNT, remained constant during the "on-off" switch process, suggesting that Zn^{2+} ions only attached onto the surface of Pd atom. When the EDTA-2Na was added into the reaction, a distinct peak at 11° appeared in the XRD, indicating that the Zn^{2+} ion was coordinated by EDTA-2Na. Then,

XPS of Pd/CNT, Pd/CNT + Zn^{2+} and Pd/CNT + Zn^{2+} + EDTA-2Na were also recorded (Figs. 9b and 9c). After addition of Zn^{2+}, there is

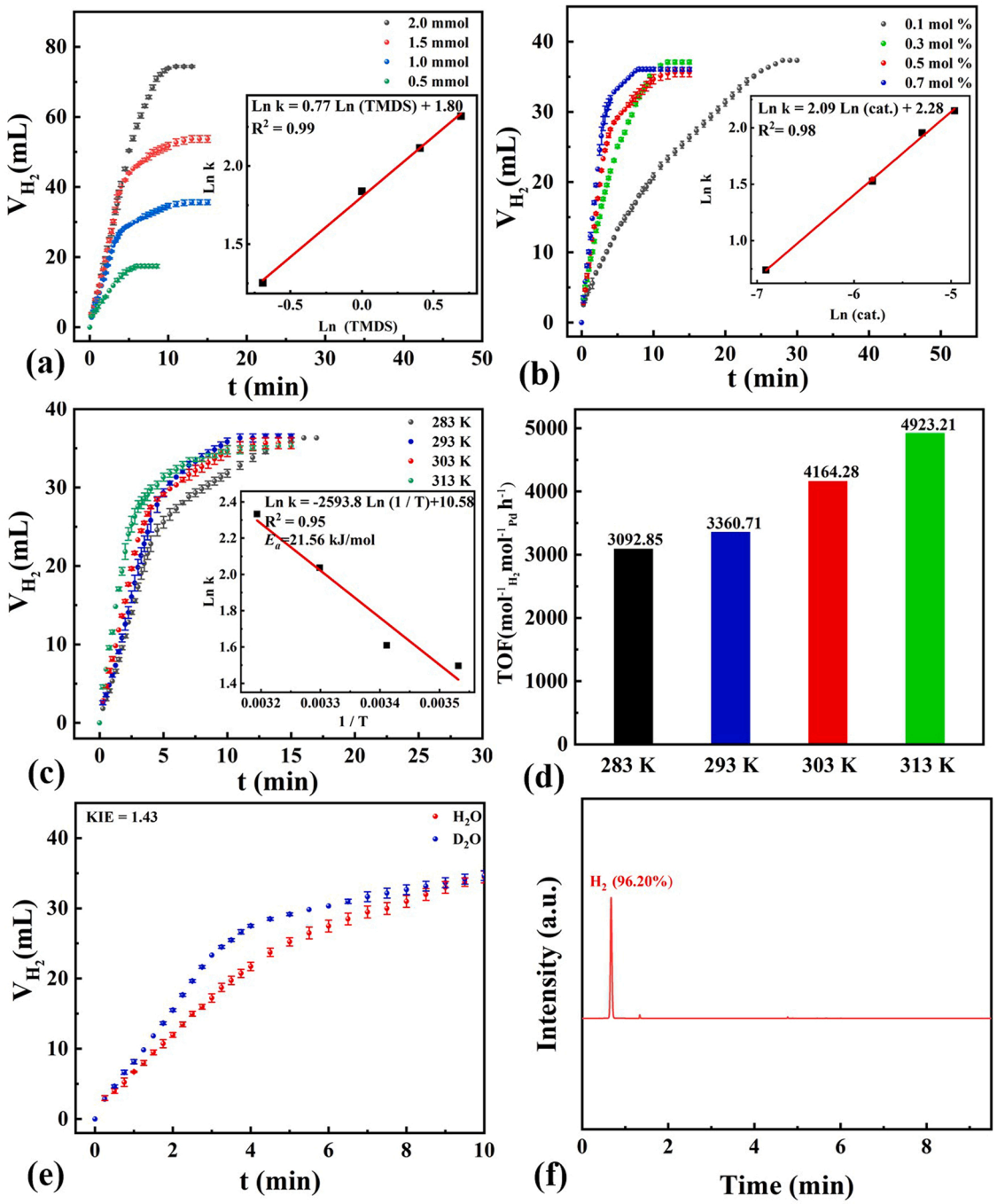

Fig. 5. The volume plots of obtained H_2 gas vs. time for the hydrolysis of Si-H bond with (a) different concentrations of (a) initial tetramethyldisiloxane, (b) Pd/CNT and (c) at various reaction temperatures; (d) the corresponding TOF value at various reaction temperatures, (e) H_2 evolution upon the hydrolysis of Si-H bond in H_2O (red) or D_2O (black); (f) GC spectra of obtained gas from the hydrolysis of Si-H bond over Pd/CNT at 30 °C.

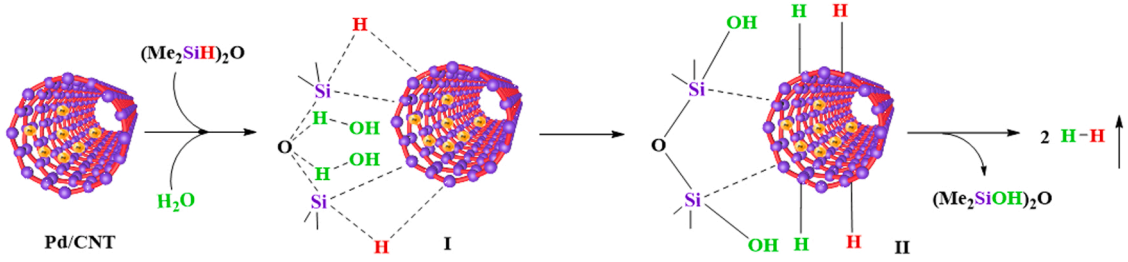

Scheme 2. The proposed mechanism for the hydrolysis of Si-H bond over Pd/CNT.

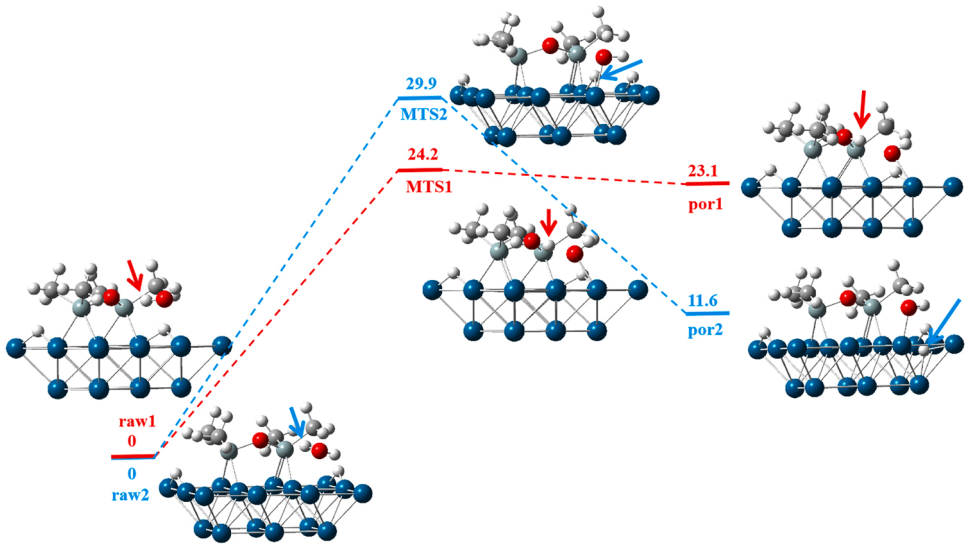

Fig. 6. Two plausible mechanism pathways of the cleavage of the O-H bond in water.

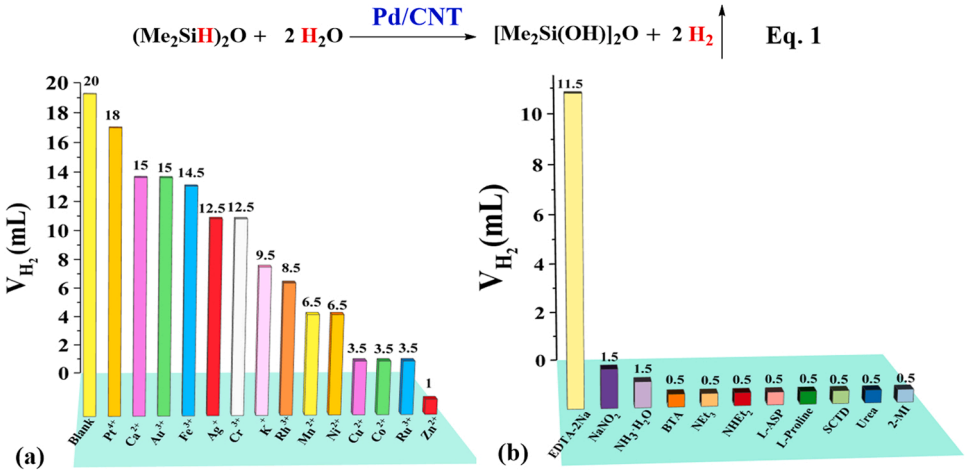

Fig. 7. (a) The volume of obtained H_2 gas in 2 min of the hydrolysis of Si-H bond over Pd/CNT after the addition of various metal cations, (b) ligands. Reaction condition: 2 mmol of TMDS, 5×10^{-3} mmol of Pd/CNT, 2.5×10^{-3} mmol of metal cations or ligands (0.01 mmol) in the mixture of 1,4-dioxane (1 mL) and water (1 mL) at 30 °C.

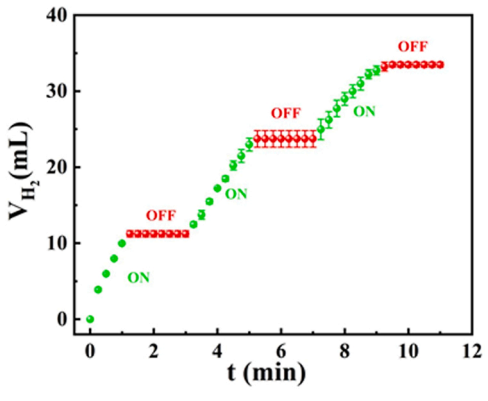

Fig. 8. "On-off" control of H_2 evolution upon the hydrolysis of Si-H bond. Reaction condition: 2 mmol of TMDS, 5×10^{-3} mmol of Pd/CNT in the mixture of 1,4-dioxane (1 mL) and water (1 mL) at 30 °C.

an obvious shift in the Pd 3d of Pd/CNT compared to fresh Pd/CNT, indicating a strong electronic interaction between the Pd atom and Zn^{2+} ion at the surface of CNT. It appears that Zn^{2+} ions located and attached onto the surface of Pd atoms, inhibit the surface-active sites, resulting in H_2 evolution switch off. After the addition of EDTA-2Na, the shift of Pd 3d disappears in the XPS (Fig. 9b), while a right shift in the Zn 2p appear (Fig. 9c), indicating that Zn^{2+} ions are removed from Pd atoms due to the strong coordination ability of EDTA-2Na, resulting in H_2 evolution switch on. Fig. 9c shows that Zn (II) remains unchanged during the"on-off"switch process as observed by its superior negative φ^{θ} (−0.78 V), confirming the absence of redox reaction.

3.6. *The mechanistic insights into the "on-off" switch*

To provide mechanistic insights into the "on-off" switch upon operating the Zn^{2+}/EDTA-2Na system, for on-demand H_2 evolution upon the hydrolysis of Si-H bond, a systematic density functional theory (DFT) calculation was also performed. Given the fact that the on-demand H_2 evolution is occurring at the surface of PdNPs, it is essential to study the adsorption of H* at the surface of the Pd/CNT. To accurately simulate the Pd (111) surface, four-layer slab and six-layer slab were enclosed in a

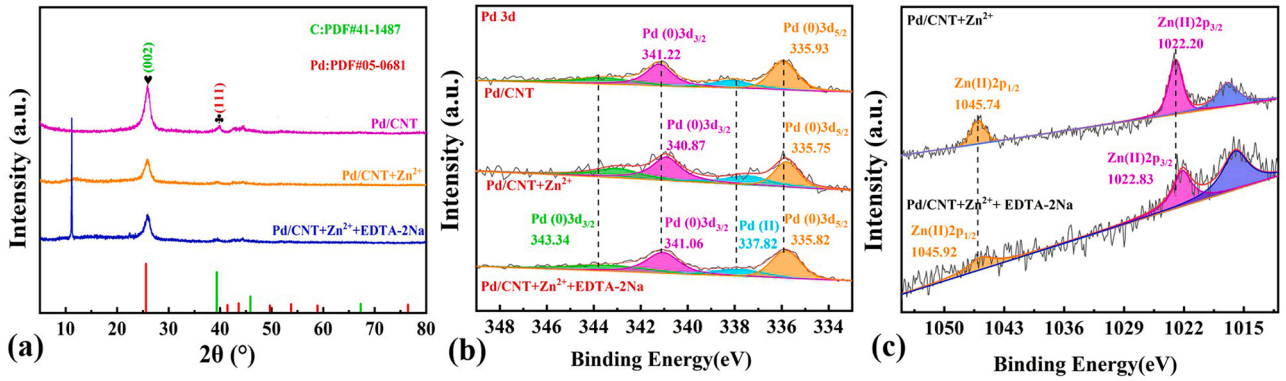

Fig. 9. (a) XRD, (b) Pd 3d, (c) Zn 2p XPS patterns of Pd/CNT, Pd/CNT + Zn^{2+} and Pd/CNT + Zn^{2+} + EDTA-2Na.

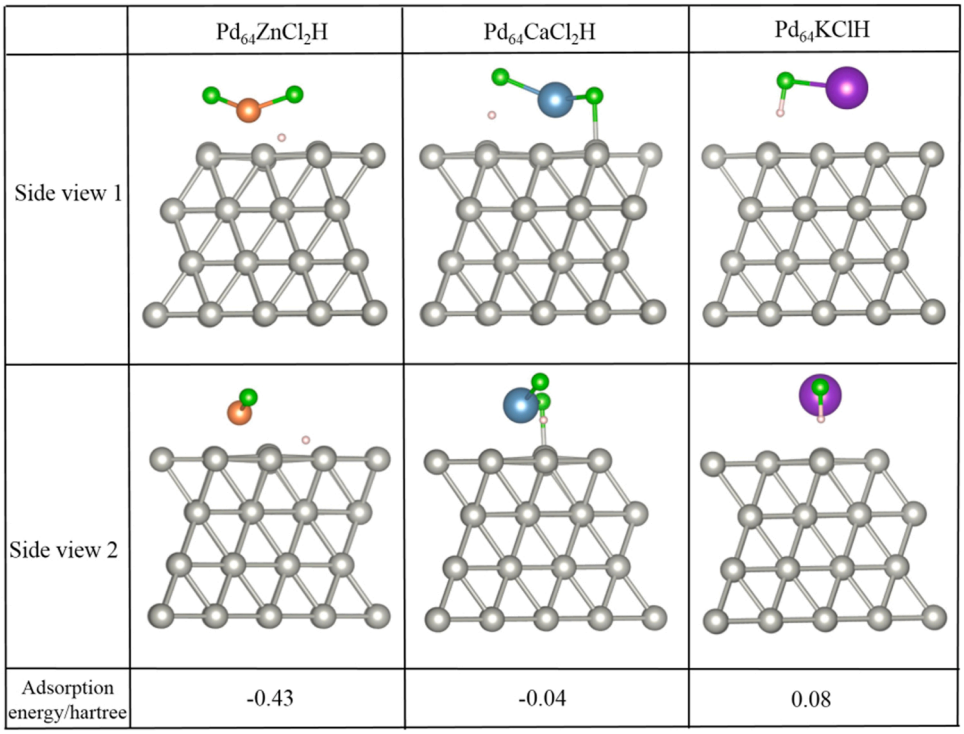

Fig. 10. The optimize structures of H adsorbed on $Pd_{64}ZnCl_2$, $Pd_{64}CaCl_2$ and $Pd_{64}KCl$ with adsorption energy nearest to zero from two view sides.

super-cell with a sufficiently large vacuum region of 10 Å to ensure the periodic images to be well separated. During the geometry optimization of four-layer slab and six-layer slab of Pd models, the atoms in the bottom two layers were fixed, and the rest of the atoms were allowed to relax in order to decrease the complexity of calculation, and we used the k-point meshes of 4 × 4 × 1. Structural optimization was performed until the Hellmann-Feynman forces acting on each atom were less than 0.02 eV/Å. Atoms position almost unchanged confirmed that four-layer slab model was suitable for calculation. Based on the Pd (111) model, a $ZnCl_2$, $CaCl_2$ or KCl molecule was added at the center of the top layer of Pd_{64} to build $Pd_{64}ZnCl_2$, $Pd_{64}CaCl_2$ or $Pd_{64}KCl$ models, respectively. Differential charge density of $Pd_{64}ZnCl_2$, $Pd_{64}CaCl_2$ and $Pd_{64}KCl$ models was calculated and visualized by Vesta program. [60] In the optimized structures of $Pd_{64}ZnCl_2$, $Pd_{64}CaCl_2$ and $Pd_{64}KCl$ models (Fig. S3), (i) Zn was sandwiched between 2 Cl and Pd_{64} in $Pd_{64}ZnCl_2$; (ii) three atoms of $CaCl_2$ were basically formed into a plane in $Pd_{64}CaCl_2$, which was parallel to the Pd layers; (iii) Cl was sandwiched between K and Pd_{64} in $Pd_{64}KCl$ by vertical conformation analysis.

In order to elucidate the catalytic performance of the "on-off" switch in the presence of different metal ions, the optimized structures and hydrogen absorption energy, $\Delta_{Gads(H)}$, on diversity H* adsorption sites of Pd_{64}, $Pd_{64}ZnCl_2$, $Pd_{64}CaCl_2$ and $Pd_{64}KCl$ were calculated (Fig. S4). A preferred consideration of the initial adsorption sites of H* was applied, including the top site on Pd1, B1 and B2. The top site on B11 and B22 were also considered as the adsorption sites for $Pd_{64}ZnCl_2$, $Pd_{64}CaCl_2$ and $Pd_{64}KCl$ due to asymmetrical geometry. The adsorption energy is determined as follows:

$$\Delta G_{ads}\,(H) = E_{model\text{-}H} - E_{model} - E_H$$

where $E_{model\text{-}H}$ is the individual energy of the catalyst with H* , E_{model} is the energy of the catalyst without the adsorbate, E_H is the energy of H* , $\Delta G_{ads}(H)$ is the adsorption energy of H* on Pd, respectively. Detailed energy data and optimized structures for diversity adsorption sites of Pd_{64}, $Pd_{64}ZnCl_2$, $Pd_{64}CaCl_2$ and $Pd_{64}KCl$ were obtained and are summarized in Table S1 and Fig. S5-S8. As shown in Fig. 10, H* is located between $ZnCl_2$ and Pd_{64} on the surface of $Pd_{64}ZnCl_2$ (side view **1**), but it is far away from $ZnCl_2$ (**side view 2**) indicating that H* has difficulties to contact the surface of Pd in the presence of $ZnCl_2$ due to the steric

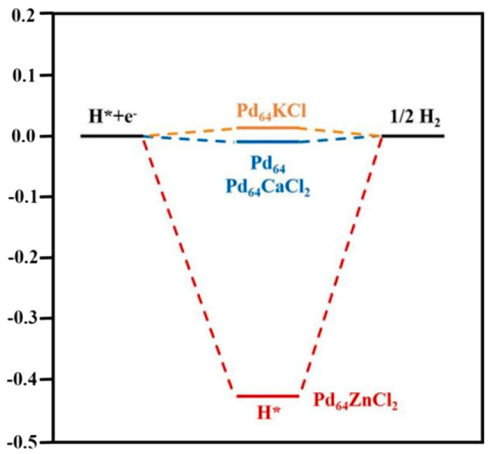

Fig. 11. The calculated free energy diagram for H adsorption.

effects. Whereas H* is located between Pd_{64} and $CaCl_2$/KCl from both side views on the surface of $Pd_{64}CaCl_2$/Pd_{64}KCl, suggesting that the adsorption capability of H* on Pd is not affected by the $CaCl_2$/KCl molecule. As displayed in Fig. 11, the Gads(H) values of Pd_{64}, $Pd_{64}CaCl_2$ and Pd_{64}KCl are − 0.05, − 0.04 and 0.08 eV, respectively, which remains close to zero. Note that the Gads(H) value of $Pd_{64}ZnCl_2$ is − 0.43 eV, indicating that desorption capacity of H* on Pd clearly decreases, and resulting in switched off of H_2 evolution.

As observed in Fig. 12, the differential charge density was also calculated to analyze $ZnCl_2$, $CaCl_2$ and KCl adding-induced electron density redistribution. The DFT results show that the electron cloud density (blue) of $Pd_{64}ZnCl_2$ is much lower than those of $Pd_{64}CaCl_2$ and Pd_{64}KCl. Thus, the electron cloud density of Pd/CNT is greatly reduced by addition of $ZnCl_2$, which disfavors the Si-H/O-H bond cleavage in the H_2 evolution upon Si-H bond hydrolysis.

In summary, the DFT results show that the contact between H* and the Pd surface in the presence of $ZnCl_2$ is difficult due to steric effects. Then, the Gads(H) value of $Pd_{64}ZnCl_2$ is − 0.43 eV, indicating that desorption capacity of H* on Pd clearly decreases. Finally, the electron cloud density of Pd/CNT is greatly reduced by addition of $ZnCl_2$ disfavoring Si-H/O-H bond cleavage in the hydrolysis of the Si-H bond, [61,62] and as a result H_2 evolution is switched off.

3.7. Recycling experiment

For the study of the future practical and industrial application of the as-synthesized Pd/CNT the durability and stability of the present Pd/CNT nanohybrid were considered, and the recycling tests were conducted (Fig. S9). The Pd/CNT nanohybrid has been separated, reobtained and used by a simple filtration after each H_2 evolution. The result showed that the heterogeneous Pd/CNT nanohybrid was successfully recycled for at least five runs without any significant decrease in activity. In addition, the 5^{th} recycled Pd/CNT nanohybrid has further been measured by XRD. As shown in Fig. S10, it is clear that the 5^{th} recycled Pd/CNT nanohybrid remains in the same crystal structure as the fresh one, indicating that the Pd/CNT nanohybrid is an excellent stable and recyclable catalyst.

4. Concluding remarks

In summary, a series of unprecedented carbon nanotubes stabilized Pd, Au, Rh, Pt and Ru nanohybrids have been employed as highly efficient nanocatalysts for the controllable H_2 evolution upon Si-H bond hydrolysis. First, the detailed physical characterizations confirmed that PdNPs are successfully stabilized at the surface of carbon nanotubes. Among them, the optimal Pd/CNT nanohybrid exhibited the highest catalytic performance, with a TOF of 4164 h^{-1}, in the H_2 evolution upon TMDS hydrolysis at 30 °C. The kinetic study, including initial TMDS concentration, amount of Pd/CNT, and reaction temperature, and

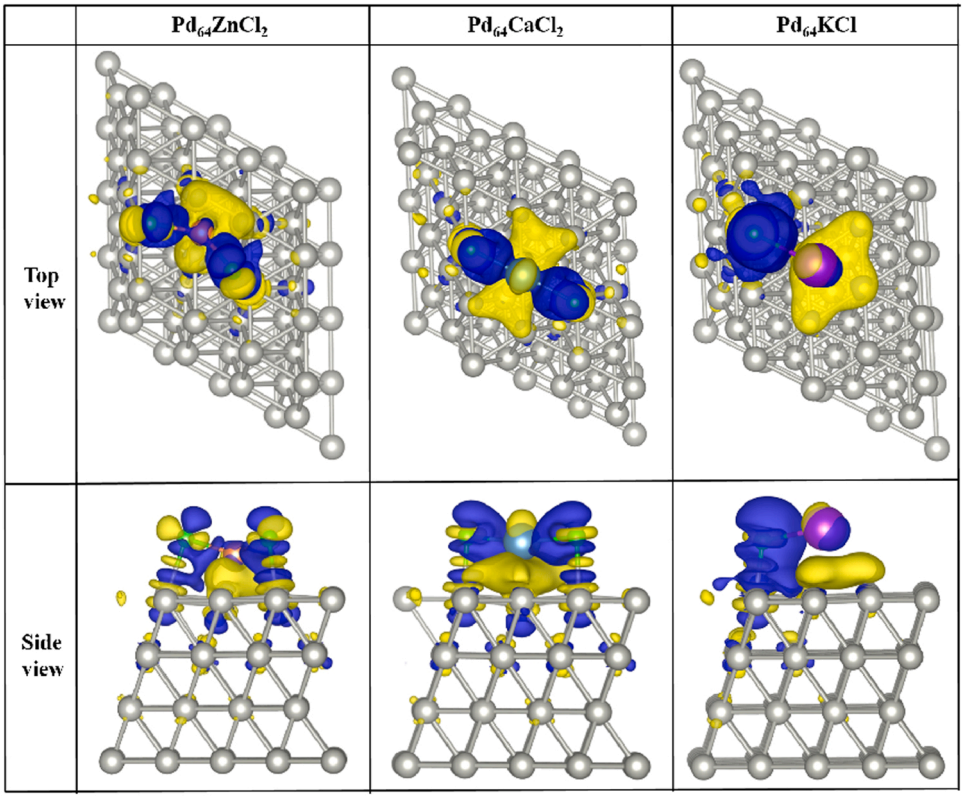

Fig. 12. differential charge densities of $Pd_{64}ZnCl_2$, $Pd_{64}CaCl_2$ and Pd_{64}KCl. yellow represents positive and blue represents negative.

detailed mechanistic investigations, particularly KIE experiments, have shown that the cleavage of the O-H bond in water is not the rate-determining step of the hydrolysis of Si-H bond; on the other hand, it favors a concerted process between Si-H oxidative addition and water O-H bond oxidative addition.

A novel and highly selective "on-off" switch, via Zn^{2+}/EDTA-2Na system, for on-demand H_2 evolution upon the hydrolysis of the Si-H bond, was successfully achieved by inhibition and activation regulation of surface-active sites on the catalyst. The detailed physical characterizations (particularly XRD and XPS) and DFT calculations confirmed that Zn^{2+} ions are located and bound at the surface of PdNPs and inhibit surface-active sites by the steric effect and strong electronic interaction between the PdNPs and Zn^{2+} ions, resulting in H_2 evolution switch off. H_2 evolution is switched on by EDTA-2Na due to its excellent coordination ability with Zn^{2+}, reactivating these surface-active sites.

This work not only provides a new chemical hydrogen storage material for efficient production, transportation and storage of H_2, but it also proposes a novel and highly selective"on-off"switch for on-demand H_2 evolution.

CRediT authorship contribution statement

Xiang Liu: Investigation, Resources, Supervision, Conceptualization, Project administration Verification, Formal analysis, Visualization, Writing - original draft, Writing - review & editing. **Xiaotao Jin**: Investigation. **Jiaying Yan**: Software, Investigation, Writing - review & editing. **Shuaiwei Fan**: Software, Investigation, Writing - review & editing. **Yanlan Wang**: Formal analysis. **Didier Astruc**: Supervision, Conceptualization, Project administration, Writing - review & editing.

Declaration of Competing Interest

The authors declare that they have no known competing financial interests or personal relationships that could have appeared to influence the work reported in this paper.

Data availability

Data will be made available on request.

Acknowledgements

Financial support from the NSFC (Nos. 21805166, 21901097 and 22108157), the 111 Project of China (No. D20015), the Outstanding Young and Middle-aged Science and Technology Innovation Teams, Ministry of Education, Hubei Province, China (T2020004), Cultivation Program for Young Innovative Talents in Shandong Provincial Colleges and Universities (Innovation Team of Functional Organometallic Materials Presided by Prof. Yanlan Wang), Université de Bordeaux and CNRS is gratefully acknowledged, thanks eceshi (www. eceshi.com) for the TEM, ICP analysis and Yuan Zhou from Shiyanjia Lab (www. shiyanjia.com) for GC test.

Appendix A. Supporting information

Supplementary data associated with this article can be found in the online version at doi:10.1016/j.apcatb.2022.122261.

References

[1] M. Yadava, Q. Xu, Liquid-phase chemical hydrogen storage materials, Energy Environ.. Sci.. 5 (2012) 9698–9725.
[2] W.-W. Zhan, Q. –L. Zhu, Q. Xu, Dehydrogenation of ammonia borane by metal nanoparticle catalysts, ACS Catal. 6 (2016) 6892–6905.
[3] Q. Sun, N. Wang, Q. Xu, J. Yu, Nanopore-supported metal nanocatalysts for efficient hydrogen generation from liquid-phase chemical hydrogen storage materials, Adv. Mater.. 32 (2020), 2001818.
[4] Q. Yao, Y. Ding, Z.-H. Lu, Recent advances in the "on-off" approaches for on-demand liquid-phase hydrogen evolution, Inorg. Chem. Front.. 7 (2020) 3837–3874.
[5] X. Liu, X. Zhang, D.-S. Li, S. Zhang, Q. Zhang, Recent advances in the "on-off" approaches for on-demand liquid-phase hydrogen evolution, J. Mater. Chem. A 9 (2021) 18164–18174.
[6] M. Huang, L. Ouyang, H. Wang, J. Liu, M. Zhu, Hydrogen generation by hydrolysis of MgH_2 and enhanced kinetics performance of ammonium chloride introducing, Int. J. Hydrog. Energ. 40 (2015) 6145–6150.
[7] M. Ma, L. Yang, L. Ouyang, H. Shao, M. Zhu, Promoting hydrogen generation from the hydrolysis of Mg-Graphite composites by plasma-assisted milling, Energy 167 (2019) 1205–1211.
[8] M. Huang, L. Ouyang, J. Ye, J. Liu, X. Yao, H. Wang, H. Shao, M. Zhu, Hydrogen generation via hydrolysis of Magnesium with seawater using Mo, MoO_2, MoO_3 and MoS_2 as catalysts, J. Mater. Chem. A 5 (2017) 8566–8575.
[9] L. Ouyang, W. Chen, J. Liu, M. Felderhoff, H. Wang, M. Zhu, Enhancing the regeneration process of consumed $NaBH_4$ for hydrogen storage, Adv. Energy Mater. 1700299 (2017).
[10] K. Chen, L. Ouyang, H. Zhong, J. Liu, H. Wang, H. Shao, Y. Zhang, M. Zhu, Converting H^+ from coordinated water into H^- enables super facile synthesis of $LiBH_4$, Green. Chem. 21 (2019) 4380–4387.
[11] F. Xu, Y. Wang, C. Wang, W. Huang, X. Liu, Dehydrogenation of hydrous hydrazine over carbon nanosphere-supported PtNi nanoparticles for on-demand H_2 release, Fuel 332 (2023), 126116.
[12] Q. Zhang, F. Xu, W. Huang, Y. Wang, X. Liu, Hydrolytic dehydrogenation of NH_3BH_3 over $Cu/CoO_x(OH)_y$ nanocomposite for H2 evolution, Fuel 335 (2023), 126870.
[13] H. Song, M. Wu, Z. Tang, J.-S. Tse, B. Yang, S. Lu, Single atom ruthenium-doped CoP/CDs nanosheets via splicing of carbon-dots for robust hydrogen production, Angew. Chem. Int. Ed. 60 (2021) 7234–7244.
[14] Y. Peng, Y. Zhang, A. Guo, M. Mao, Y. Wang, Y. Long, G. Fan, Universal low-temperature oxidative thermal redispersion strategy for green and sustainable fabrication of oxygen-rich carbons anchored metal nanoparticles for hydrogen evolution reactions, Chem. Eng. J. 433 (2022), 133648.
[15] H.-N. Abdelhamid, A review on hydrogen generation from the hydrolysis of sodium borohydride, Int. J. Hydrog. Energy 46 (2021) 726–765.
[16] R. Wei, Z. Chen, H. Lv, X. Zheng, X. Ge, L. Sun, K. Song, C. Kong, W. Zhang, B. Liu, Ultrafine RhNi Nanocatalysts Confined in Hollow Mesoporous Carbons for a Highly Efficient Hydrogen Production from Ammonia Borane, Inorg. Chem. 60 (2021) 6820–6828.
[17] T. He, P. Pachfule, H. Wu, Q. Xu, P. Chen, Hydrogen carriers, Nat. Rev. Mater. 1 (2016) 16059.
[18] A. Kumar, P. Daw, D. Milstein, Homogeneous catalysis for sustainable energy: hydrogen and methanol economies, fuels from biomass, and related topics, Chem. Rev.. 122 (2022) 385–441.
[19] H. Liu, L. Zhang, H. Ma, G. Lu, H. Luo, X. Wang, X. Huang, Z. Lan, J. Guo, Aluminum hydride for solid-state hydrogen storage: Structure, synthesis, thermodynamics, kinetics, and regeneration, J. Energy Chem. 52 (2021) 428–440.
[20] B. Zhu, R. Zou, Q. Xu, Metal-organic framework based catalysts for hydrogen evolution, Adv. Energy Mater. 8 (2018), 1801193.
[21] L. Ouyang, J. Jiang, K. Chen, M. Zhu, Z. Liu, Hydrogen production via hydrolysis and alcoholysis of light metal-based materials: a review, Nano-Micro Lett. 13 (2021) 134.
[22] C. Wang, Q. Wang, F. Fu, D. Astruc, Hydrogen generation upon nanocatalyzed hydrolysis of hydrogen-rich boron derivatives: recent developments, Acc. Chem. Res. 53 (2020) 2483–2493.
[23] C. Wang, D. Astruc, Recent developments of nanocatalyzed liquid-phase hydrogen generation, Chem. Soc. Rev. 50 (2021) 3437–3484.
[24] A.-K.L. Teo, W.-Y. Fan, A Novel Iron Complex For Highly Efficient Catalytic Hydrogen Generation From The Hydrolysis Of Organosilanes, in: Chem. Commun., 50, 2014, pp. 7191–7194.
[25] J. Zhou, W. Hou, X. Liu, D. Astruc. Pd, Rh and Ru nanohybrid-catalyzed tetramethyldisiloxane hydrolysis for H_2 generation, nitrophenol reduction and Suzuki–Miyaura cross-coupling, Inorg. Chem. Front. 9 (2022) 1416–1422.
[26] A.-G.M. Da Silva, C.-M. Kisukuri, T.-S. Rodrigues, E.-G. Candido, I.-C. de Freitas, A.-H.M. da Silva, J.-M. Assaf, D.-C. Oliveira, L.-H. Andrade, P.-H.C. Camargo, MnO_2 nanowires decorated with Au ultrasmall nanoparticles for the green oxidation of silanes and hydrogen production under ultralow loadings, Appl. Catal. B Environ.. 184 (2016) 35–43.
[27] D. Ventura-Espinosa, S. Sabater, A. Carretero-Cerdán, M. Baya, J. –A. Mata, High production of hydrogen on demand from silanes catalyzed by iridium complexes as a versatile hydrogen storage system, ACS Catal. 8 (2018) 2558–2566.
[28] J.-M. Brunel, Polysilanes: the grail for a highly-neglected hydrogen storage source, Int. J. Hydrog. Energ. 42 (2017) 23004–23009.
[29] T. Mitsudome, T. Urayama, T. Kiyohiro, Z. Maeno, T. Mizugaki, K. Jitsukawa, K. Kaneda, On-demand hydrogen production from organosilanes at ambient temperature using heterogeneous gold catalysts, Sci. Rep. 6 (2016) 37682.
[30] J. Pesti, G.-L. Larson, Tetramethyldisiloxane: a practical organosilane reducing agent, Org. Process Res. Dev. 20 (2016) 1164–1181.
[31] N. Asao, Y. Ishikawa, N. Hatakeyama, Y. Yamamoto, M. Chen, W. Zhang, A. Inoue, Nanostructured materials as catalysts: nanoporous-gold-catalyzed oxidation of organosilanes with water, Angew Chem. Int. Ed. 49 (2010) 10093–10095.
[32] J. John, E. Gravel, A. Hagège, H. Li, T. Gacoin, E. Doris, Catalytic oxidation of silanes by carbon nanotube–gold nanohybrids, Angew. Chem. Int. Ed. 50 (2011) 7533–7536.

[33] Z. Chen, Q. Zhang, W. Chen, J. Dong, H. Yao, X. Zhang, X. Tong, D. Wang, Q. Peng, C. Chen, W. He, Y. Li, Single-Site Au^{I} catalyst for silane oxidation with water, Adv. Mater. 30 (2018), 1704720.
[34] C. Wang, W.-J. Teo, S. Ge, Access to stereodefined (*Z*)-allylsilanes and (*Z*)-allylic alcohols via cobalt-catalyzed regioselective hydrosilylation of allenes, Nat. Commun. 8 (2017) 2258.
[35] J. Tönjes, L. Longwitz, T. Werner, Poly(methylhydrosiloxane) as a reductant in the catalytic base-free Wittig reaction, Green. Chem. 23 (2021) 4852–4857.
[36] J. John, E. Gravel, A. Hagège, H. Li, T. Gacoin, E. Doris, Catalytic oxidation of silanes by carbon nanotube–gold nanohybrids, Angew. Chem. Int. Ed. 50 (2011) 7533–7536.
[37] D. Ventura-Espinosa, A. Carretero-Cerdán, M. Baya, H. García, J. –A. Mata, Catalytic dehydrogenative coupling of hydrosilanes with alcohols for the production of hydrogen on-demand: application of a silane/alcohol pair as a liquid organic hydrogen carrier, Chem. Eur. J. 23 (2017) 10815–10821.
[38] W. Sattler, G. Parkin, Zinc catalysts for on-demand hydrogen generation and carbon dioxide functionalization, J. Am. Chem. Soc. 134 (2012) 17462–17465.
[39] R. Murugavel, A. Voigt, M.-G. Walawalkar, H.-W. Roesky, Hetero- and metallasiloxanes derived from silanediols, disilanols, silanetriols, and trisilanols, Chem. Rev. 96 (1996) 2205–2236.
[40] S.-E. Denmark, C.-S. Regens, Palladium-catalyzed cross-coupling reactions of organosilanols and their salts: practical alternatives to boron- and tin-based methods, Acc. Chem. Res. 41 (2008) 1486–1499.
[41] Z. Lin, L.-C. Beltran, Z.-A. De los Santos, Y. Li, T. Adel, J.-A. Fagan, A.-R. Hight Walker, E.-H. Egelman, M. Zheng, DNA-guided lattice remodeling of carbon nanotubes, Science 37 (2022) 535–539.
[42] R. Nandan, G. Raj, K.-K. Nanda, FeCoNiMnCr high-entropy alloy nanoparticle-grafted ncnts with promising performance in the ohmic polarization region of fuel cells, ACS Appl. Mater. Inter. 14 (2022) 16108–16116.
[43] S.-V. Sawant, A. –W. Patwardhan, J.-B. Joshi, K. Dasgupta, Boron doped carbon nanotubes: Synthesis, characterization and emerging applications – a review, Chem. Eng. J. 427 (2022), 131616.
[44] P. Michaud, D. Astruc, J.-H. Ammeter, Electron-transfer pathways in the reduction of d_6 and d_7 organo-iron cations by $LiAlH_4$ and $NaBH_4$, J. Am. Chem. Soc. 104 (1982) 3755–3757.
[45] Z.-T. Liu, C.-X. Wang, Z.-W. Liu, J. Lu, Selective hydrogenation of cinnamaldehyde over Pt-supported multi-walled carbon nanotubes: Insights into the tube-size effects, Appl. Catal. A Gen. 344 (2008) 114–123.
[46] L. Zhang, J. Liang, L. Yue, Z. Xu, K. Dong, Q. Liu, Y. Luo, T. Li, X. Cheng, G. Cui, B. Tang, A. –A. Alshehri, K.-A. Alzahrani, X. Guo, X. Sun, N-doped carbon nanotubes supported $CoSe_2$ nanoparticles: A highly efficient and stable catalyst for H_2O_2 electrosynthesis in acidic media, Nano Res 15 (2022) 304–309.
[47] G. Povie, Y. Segawa, T. Nishihara, Y. Miyauchi, K. Itami, Synthesis of a carbon nanobelt, Science 356 (6334) (2017) 172–175.
[48] S.-D. Perera, R.-G. Mariano, K. Vu, N. Nour, O. Seitz, Y. Chabal, K.-J. Balkus, Hydrothermal synthesis of graphene-TiO_2 nanotube composites with enhanced photocatalytic activity, ACS Catal. 2 (2012) 949–956.
[49] A. Islam, S.-H. Teo, M.-R. Awual, Y.-H. Taufiq-Yap, Assessment of clean H_2 energy production from water using novel silicon photocatalyst, J. Clean. Prod. 244 (2020), 118805.
[50] J. Chang, L. Feng, C. Liu, W. Xing, X. Hu, An Effective Pd–Ni_2P/C anode catalyst for direct formic acid fuel cells, Angew. Chem. Int. Ed. 53 (2014) 122–126.
[51] F. Fu, C. Wang, Q. Wang, A.-M. Martinez-Villacorta, A. Escobar, H. Chong, X. Wang, S. Moya, L. Salmon, E. Fouquet, J. Ruiz, D. Astruc, Highly selective and sharp volcano-type synergistic Ni_2Pt@ZIF-8-catalyzed hydrogen evolution from ammonia borane hydrolysis, J. Am. Chem. Soc. 140 (2018) 10034–10042.
[52] M. –J. Frisch, G.-W. Trucks, H.-B. Schlegel, G. –E. Scuseria, M.-A. Robb, J.-R. Cheeseman, G. Scalmani, V. Barone, G.-A. Petersson, H. Nakatsuji, X. Li, M. Caricato, A.-V. Marenich, J. Bloino, B. –G. Janesko, R. Gomperts, B. Mennucci, H.-P. Hratchian, J. –V. Ortiz, A.-F. Izmaylov, J.-L. Sonnenberg, Williams F. Ding, F. Lipparini, F. Egidi, J. Goings, B. Peng, A. Petrone, T. Henderson, D. Ranasinghe, V.-G. Zakrzewski, J. Gao, N. Rega, G. Zheng, W. Liang, M. Hada, M. Ehara, K. Toyota, R. Fukuda, J. Hasegawa, M. Ishida, T. Nakajima, Y. Honda, O. Kitao, H. Nakai, T. Vreven, K. Throssell, J.A. Montgomery, J.E. Peralta, F. Ogliaro, M.-J. Bearpark, J.-J. Heyd, E.-N. Brothers, K.-N. Kudin, V.-N. Staroverov, T.-A. Keith, R. Kobayashi, J. Normand, K. Raghavachari, A.-P. Rendell, J.-C. Burant, S.-S. Iyengar, J. Tomasi, M. Cossi, J.-M. Millam, M. Klene, C. Adamo, R. Cammi, J.-W. Ochterski, R.-L. Martin, K. Morokuma, O. Farkas, J.-B. Foresman, D.-J. Fox, Gaussian 16, Revision C.01, Gaussian. Inc., Wallingford CT, 2016.
[53] C. Luo, F. Fu, X. Yang, J. Wei, C. Wang, J. Zhu, D. Huang, D. Astruc, P. Zhao, Highly efficient and selective Co@ZIF-8 nanocatalyst for hydrogen release from sodium borohydride hydrolysis, ChemCatChem 11 (2019) 1643–1649.
[54] Q. Wang, F. Fu, S. Yang, M. Martinez Moro, M. d l A. Ramirez, S. Moya, L. Salmon, J. Ruiz, D. Astruc, Dramatic synergy in CoPt nanocatalysts stabilized by "click" dendrimers for evolution of hydrogen from hydrolysis of ammonia borane, ACS Catal. 9 (2019) 1110–1119.
[55] F. Xu, X. Liu, "On–off" control for on-demand hydrogen production from the dehydrogenation of formic acid, ACS Catal. 11 (2021) 13913–13920.
[56] W. Huang, X. Liu, The "on-off" switch for on-demand H_2 evolution from hydrous hydrazine over Ni_8Pt_1/C nano-catalyst, Fuel 315 (2022), 123210.
[57] F. Xu, W. Huang, Y. Wang, D. Astruc, X. Liu, Efficient and controlled H_2 release from sodium formate, Inorg. Chem. Front. 9 (2022) 3514–3521.
[58] W. Huang, F. Xu, D.-S. Li, D. Astruc, X. Liu, "On-off" switch for H_2 and O_2 generation from HCOOH resp. H_2O_2, Carbon Energy (2022), https://doi.org/10.1002/cey2.269.
[59] C. Wang, J. Tuninetti, Z. Wang, C. Zhang, R. Ciganda, L. Salmon, S. Moya, J. Ruiz, D. Astruc, Hydrolysis of ammonia-borane over Ni/ZIF-8 nanocatalyst: high efficiency, mechanism, and controlled hydrogen release, J. Am. Chem. Soc. 139 (2017) 11610–11615.
[60] K. Momma, F. Izumi, VESTA 3 for three-dimensional visualization of crystal, volumetric and morphology data, J. Appl. Crystallogr 44 (2011) 1272–1276.
[61] Q.-Y. Bi, J.-D. Lin, Y.-M. Liu, H.-Y. He, F.-Q. Huang, Y. Cao, Dehydrogenation of formic acid at room temperature: boosting palladium nanoparticle efficiency by coupling with pyridinic-nitrogen-doped carbon, Angew Chem. Int. Ed. 55 (2016) 11849–11853.
[62] S. Jones, J. Qu, K. Tedsree, X.-Q. Gong, S.-C.E. Tsang, Prominent electronic and geometric modifications of palladium nanoparticles by polymer stabilizers for hydrogen production under ambient conditions, Angew. Chem. Int. Ed. 51 (2012) 11275–11278.